JACS
JOURNAL OF THE AMERICAN CHEMICAL SOCIETY
Article
pubs.acs.org/JACS

Cation-Dependent Hierarchical Assembly of U60 Nanoclusters into Macro-Ion Assemblies Imaged via Cryogenic Transmission Electron Microscopy

Jennifer A. Soltis,[†,∥] Christine M. Wallace,[‡] R. Lee Penn,[*,†] and Peter C. Burns[*,‡,§]

[†]Department of Chemistry, University of Minnesota, Minneapolis, Minnesota 55455, United States

[‡]Department of Civil & Environmental Engineering & Earth Sciences, University of Notre Dame, Notre Dame, Indiana 46556, United States

[§]Department of Chemistry and Biochemistry, University of Notre Dame, Notre Dame, Indiana 46556, United States

Supporting Information

ABSTRACT: Self-assembly of $([UO_2(O_2)OH]_{60})^{60-}$ (U60), an actinide polyoxometalate with fullerene topology, can be induced by the addition of mono- and divalent cations to aqueous U60 solutions. Dynamic light scattering and small-angle X-ray scattering lend important insights into assembly in this system, but direct imaging of U60 and its assemblies via transmission electron microscopy (TEM) has remained an elusive goal. In this work, we used cryogenic TEM to image U60 and secondary and tertiary assemblies of U60 to characterize the size, morphology, and rate of formation of the secondary and tertiary structures. The kinetics and final morphologies of the secondary and tertiary structures strongly depend on the cation employed, with monovalent cations (Na^+ and K^+) leading to the highest rates and largest secondary and tertiary structures.

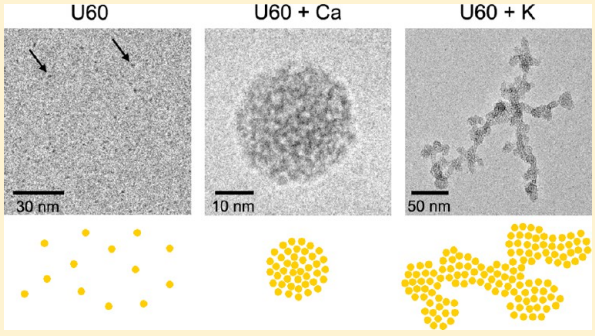

INTRODUCTION

Nuclear power plants produce approximately 12% of electricity worldwide, and there is a pressing need for safe storage and reprocessing of spent nuclear fuel.[1] Nuclear fuel rods have a usable lifetime of approximately 18 months, after which they must be stored in cooling pools for several years until the heat-producing nuclear reactions have decreased to a level appropriate for long-term storage.[1] The cladding on nuclear fuel rods is intended to prevent direct contact of uranium and its fission byproducts with the water of cooling pools. However, cladding failure has resulted in the deposition of uranium oxide minerals, such as studtite.[2] Uranium minerals can also precipitate when fuel and fuel waste interact with ion-rich groundwater (e.g., leakage from Hanford's waste storage tanks)[3] and seawater (e.g., at Fukushima).[4]

Over the past decade, a family of uranyl peroxide clusters has been synthesized and characterized.[5] In each of these, the exterior surface is truncated by the relatively unreactive oxygen atoms of the uranyl ions, which is consistent with their designation as polyoxometalates (POMs).[5a] Most of these U-POMs are cage clusters, and many have fullerene topologies. The family includes rings, bowls, and core−shell topologies. Peroxide in these clusters bridges uranyl ions, with the peroxide bidentate to uranyl. A variety of other bridges are also incorporated into such clusters, including pyrophosphate, oxalate, nitrate, phosphate, and hydroxyl. Actinide POMs and peroxide clusters are not limited to U, with one neptunyl peroxide cluster and a variety of Th, U, Np, and Pu oxide-bearing clusters that do not contain peroxide reported.[5a] Though these clusters were all synthesized in laboratory settings and nonlaboratory actinide POMs have not yet been observed, it may be possible for actinide POMs to form where water interacts with nuclear materials, especially where radiation fields are high enough to produce substantial amounts of peroxide by radiolysis of water.[5b,6] Many POMs behave as dissolved aqueous complexes,[7] so the possibility of uranium POMs entering the groundwater or drinking water supply is of particular concern to public and environmental health.

POMs have an array of physical properties that make them attractive as building blocks for functional nanomaterials in a wide range of fields, including sensing, catalysis, magnetism, and biomedicine.[8] They are significant in part because they permit the study of well-structured clusters and size-property relations, and transition metal POMs (TM-POMs) have been studied for over 100 years.[9] POMs are sometimes called macroanions because of their overall negative charge and large size compared with other polyatomic anions.[7] They can undergo several levels of hierarchical self-assembly, and increased control over self-assembly in POMs could enable the development of new materials, including nanostructured nuclear fuels.[5b,8b,10]

Received: September 17, 2015
Published: December 28, 2015

DOI: 10.1021/jacs.5b09802
J. Am. Chem. Soc. 2016, 138, 191−198

POMs provide a unique opportunity to study aggregation of nanometer-scale clusters in aqueous solutions. For U-POMs in particular, the high electron count of uranium provides excellent contrast with water in electron and X-ray scattering experiments. Large (1−5 nm) macroanions in solution can spontaneously self-assemble into larger but still nanoscale objects, and such assemblies remain stable in solution over time. Some macroanions assemble spontaneously, while others require the addition of cations or a change in the solvent composition. One type of assembly that is often observed is a hollow-shell spherical structure called a blackberry.[11] Examples of POM blackberries include $[Mo_{72}Fe_{30}]$,[12] $[Mo_{132}]$,[13] $[Cu_{20}P_8W_{48}]$,[14] $[Mo_{154}]$,[15] and $[U_{60}]$.[16] They have been observed in both aqueous[12a,14−16] and mixed-solvent systems.[13]

$([UO_2(O_2)OH]_{60})^{60-}$ (U60), shown in Figure 1, is a U-POM nanocluster consisting of 60 uranyl peroxide hydroxide

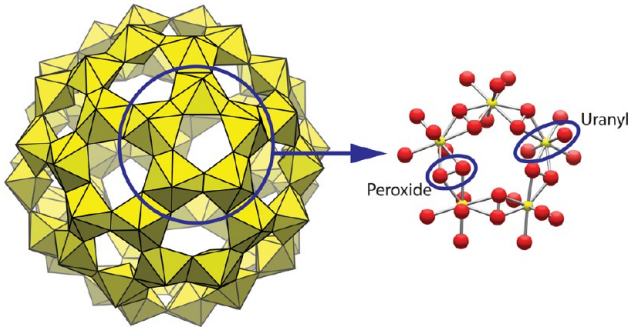

Figure 1. (left) Polyhedral representation of a U60 nanocluster. Hexagonal bipyramids have U(VI) at their centers and O at all vertices. (right) Ball-and-stick representation of a pentagonal ring composed of five bipyramidal subunits. Peroxide oxygens form bridges between subunits. Uranyl oxygens point toward the interior and exterior of the cluster. Oxygen atoms are shown in red and uranium atoms in yellow.[5b,c]

hexagonal bipyramids assembled into a fullerene topology with a diameter of 2.43 nm (as measured between the centers of bounding oxygen atoms).[5c] K^+ and Li^+ counterions are also associated with the nanocluster, with specific stoichiometries that depend on the solution pH and concentration. Each U^{6+} ion is present as a typical approximately linear uranyl (UO_2^{2+}) ion, and each of these linear ions is coordinated by two bidentate peroxide groups and two hydroxyl groups, which together define the equatorial vertices of a hexagonal bipyramid capped by the uranyl oxygen atoms.[5b,c] U60 was selected because it can be produced in high purity and because it is the most symmetrical of the family of uranyl peroxide clusters.[5c] U60 blackberry assembly can be induced by addition of cations,[16] and the size and rate of assembly are cation-dependent, although trends are difficult to predict.[16] Recent work suggests that the U60 blackberry size is inversely related to the hydrated ionic radius of the added group I cation, with the exception of Li^+ and Na^+, for which no formation of blackberries was observed at the salt concentrations studied.[16]

Blackberry POMs have been detected in solution but have not been directly imaged in situ. Small-angle X-ray scattering (SAXS) and dynamic and static light scattering (DLS and SLS) have been used to characterize the average size of blackberries in situ in solution.[6,7,11−13,17] However, direct imaging of both TM- and U-POM blackberries is particularly difficult. Imaging techniques with the appropriate resolution, such as electron microscopy, generally require high vacuum and are incompatible with liquid specimens. In fact, it was an early attempt to image molybdenum blue assemblies in a scanning electron microscope that provided evidence that they are hollow. Spheres were observed by imaging in low-vacuum environmental mode, which then burst upon exposure to high vacuum, thwarting higher-resolution imaging.[10] Drying can cause blackberries to collapse, disassemble, or aggregate in ways not representative of their in aqua state, which means that transmission electron microscopy (TEM) images of dried specimens cannot show the structural details of nanocluster assemblies.[16−18]

An alternate approach is to use cryogenic TEM (cryo-TEM). Vitrified cryo-TEM specimens preserve the in situ sample conformation and prevent artifacts induced by drying. The technique has been successfully used to study the dynamics of nanoparticle aggregation, disaggregation, and growth[19] as well as the aggregation state under reactive conditions.[20] In this study, we used cryo-TEM to probe the cation-dependent assembly of U60 nanoclusters in the presence of group I and group II cations. We present the first direct in situ observation of U-POM primary, secondary (blackberries), and tertiary structures and show that the structure size and morphology are cation-dependent.

MATERIALS AND METHODS

Synthesis. All of the solutions were prepared with ultrapure water (Millipore, 18.2 MΩ·cm resistivity). U60 nanoclusters were synthesized under ambient conditions by mixing 1 mL of 0.5 M aqueous uranyl nitrate (International Bioanalytical Industries, Inc.), 0.25 mL of 0.4 M potassium chloride, and 1 mL of 30% hydrogen peroxide in a 20 mL glass vial. The pH was adjusted to approximately 9 by the repeated addition of 2.38 M lithium hydroxide in 50 μL aliquots to a total of 0.750 mL. The gradual addition of base, with swirling and shaking between additions, is critical for proper U60 cluster formation. The vials were allowed to sit open in air for 7−10 days or more until crystals of U60 clusters formed.[5c] The cubic yellow crystals were recovered from the mother liquor and redissolved into ultrapure water to obtain monodisperse solutions.

Ultrasmall- and Small-Angle X-ray Scattering. Ultrasmall-angle X-ray scattering (USAXS) and pinhole SAXS data were collected at beamline 15-ID at the Advanced Photon Source, Argonne National Laboratory. The q range of the USAXS + pinhole SAXS system is 0.001−1.2 $Å^{-1}$, and therefore, sizes from ∼1 nm to over 1 μm can be resolved.[21] USAXS and pinhole SAXS data were collected sequentially and merged into a single dataset with an overall q range of 0.001−1.2 $Å^{-1}$. Merged data were plotted as log(intensity) versus log(q) and fitted using the Irena SAS package.[21,22]

Samples were doubly encapsulated in two Kapton capillaries, the ends of which were sealed with epoxy. Water loaded into identical capillaries was used for background measurements. Each sample type was prepared in triplicate. U60-bearing aqueous solutions were prepared by adding harvested crystals to water to achieve a concentration of 85 mg/mL. The nitrate of each target cation was added to 0.75 mL aliquots of the U60-bearing solution. Target salt concentrations were optimized to produce aggregates that persisted in solution for at least 1 week, and aggregate sizes were monitored by DLS during this process (details are provided in Table S1 in the Supporting Information). Samples were prepared at the University of Notre Dame and loaded into Kapton capillaries before shipment to the Advanced Photon Source. SAXS data were collected 6 days after preparation of the samples.

Imaging. Cryo-TEM specimens of U60 solutions were prepared using 200 mesh copper grids coated with lacy carbon film (SPI Supplies) that had been glow-discharged for 60 seconds in a Pelco glow discharger. The salts used in the imaging experiments were sodium nitrate (J. T. Baker), magnesium nitrate (Fisher), potassium

DOI: 10.1021/jacs.5b09802
J. Am. Chem. Soc. 2016, 138, 191−198

nitrate (Fisher), and calcium nitrate (Macron). Small volumes of each cation solution were added to separate 0.75 mL aliquots of 1.0 mg/mL (crystals/water) U60 with shaking. Time zero was designated as the time of cation addition. The relative differences in concentration among the cations (e.g., $[Na^+]$:$[Mg^{2+}]$) were the same as for the SAXS experiments. The final salt concentrations are listed in Table S1. No more than 20 μL of any cation solution was added to a U60 aliquot so that the concentration of U60 would be minimally affected.

A lower concentration of U60 was used for cryo-TEM than for SAXS so that the nanocluster concentration would not be too dense for imaging. At specified times, 3 μL aliquots were removed and applied to the carbon side of a TEM grid that had been loaded into a Vitrobot automated plunge freezer (FEI Mark IV). The grid was then blotted with filter paper for 2 s (−2 mm offset), allowed to relax for 1 s, and plunged into liquid ethane. The typical thickness of a vitrified film was several hundred nanometers. The vitrified specimen was then transferred to a storage box under liquid nitrogen. The time recorded was the time between cation addition and vitrification, as determined by the instant the grid was plunged into the ethane. All further handling was performed under liquid nitrogen to maintain cryogenic conditions.

Specimens with no added cations were also prepared by vitrifying aliquots of both fresh and aged U60 solutions (1.0 mg/mL crystals/water). The aged solution had been stored at high concentration (59 mg/mL crystals/water) at room temperature for 7 months prior to dilution to 1 mg/mL several hours before vitrification.

Imaging was performed using an FEI Tecnai G^2 F30 field-emission-gun transmission electron microscope equipped with a cryo stage and a Gatan UltraScan camera and operated at 300 keV under low-dose conditions. Images were collected with Digital Micrograph version 3 and processed with ImageJ version 1.48q (a public domain image processing and analysis program from the National Institutes of Health[23]). Photoshop CS2 was used for montage layouts. Images were altered by cropping and/or linear adjustments of brightness and contrast only.

Image Analysis. TEM images are, by nature, two-dimensional representations of three-dimensional objects, which means that clusters may appear to overlap or be entirely hidden by others in the projected image. Because of this, the quantity of U60 clusters per blackberry was calculated from the structure size and not by counting individually discernible clusters in the TEM images.

Major and minor axis lengths of blackberries were measured by assigning corresponding ellipses in ImageJ. Nonelliptical structures, below called "tertiary structures," were measured by assigning individual ellipses to each elliptical area of the structure. All of the reported lengths refer to the average major axis length with one standard deviation. The differences in average major axis length were compared using a one-tailed, homoscedastic (two-sample, equal variance) t test to determine statistical significance.

Surface area (S) was calculated assuming a prolate ellipsoid (two minor axes of equal length) using the approximation

$$S \approx 4\pi\left[\frac{2(ab)^{1.6} + (bb)^{1.6}}{3}\right]^{1/1.6}$$

where a and b are the lengths of the major and minor semiaxes, respectively.

The diameters of 30 individual U60 clusters were measured with the line tool, and the average diameter of 2.5 ± 0.3 nm is in close agreement with the exterior diameter measurement of 2.43 nm from single-crystal X-ray diffraction.[5c]

The spacing between assembled clusters within a blackberry was taken from the average center-to-center distance between clusters within a blackberry as calculated from SAXS measurements. Corresponding values for each of the four cations were used; these measurements ranged from 2.7 to 3.0 nm (Table S2). The cross-sectional area of an individual nanocluster was modeled as a circle using the center-to-center distance as the cluster diameter. An approximate number of U60 nanoclusters per blackberry was calculated by dividing the total surface area of a blackberry by this cross section and multiplying by ρ, the packing density of identical circles on a spherical surface. The packing density depends on the size of the circles and sphere, and exact solutions are often nontrivial, so ρ = 0.90690 for packing on the surface of an infinite sphere was used to provide an upper limit to the number of nanoclusters in secondary and tertiary structures.[24] Adjustments to account for the elimination of surface area at the interface between adjacent blackberries in a tertiary structure were omitted from the calculations, again providing an upper limit on the number of nanoclusters per structure.

Nomenclature. Samples are labeled with the cation used to induce blackberry formation. For example, a Mg-U60 blackberry is composed of U60 nanoclusters that formed after addition of $Mg(NO_3)_2$(aq).

RESULTS

Small-Angle X-ray Scattering. Data from SAXS measurements demonstrate the formation of secondary structures and the presence of isolated U60 clusters in U60 solutions after the addition of solutions of group I and group II nitrates (Figure 2). The final concentration of the added nitrates was tuned to achieve assembly in the time frame of our studies (Table S1), and no assembly was observed with added Li; as such, comparison of the sizes of the resulting secondary structures derived from the scattering data is of limited value.

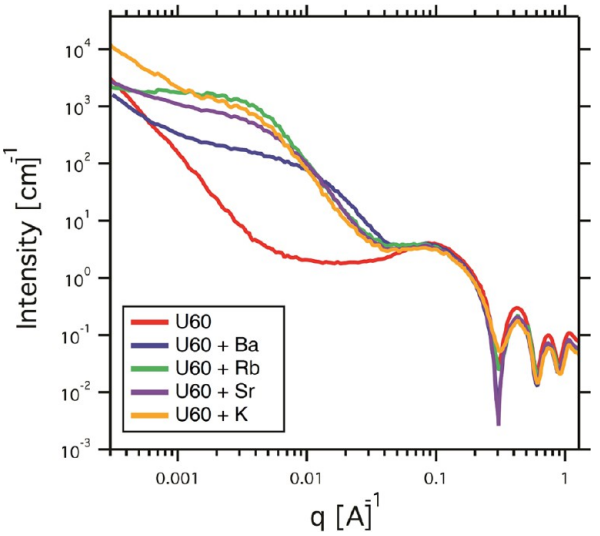

Figure 2. USAXS and pinhole SAXS data for aqueous solutions containing 85 mg/mL dissolved U60 crystals and additional group I and group II cations. Details of solution compositions are provided in the Supporting Information.

The scattering data confirm that U60 clusters persist after the onset of blackberry formation. These data were also used to determine the interaction distances between U60 clusters within the blackberries. U60 nanoclusters in crystals containing K^+ and Li^+ counterions have hard-sphere radii of 2.68 nm. The corresponding values for U60 solutions with added cations range from 2.47 to 3.15 nm (Table S2). Thus, the scattering data indicate that the center-to-center distances of U60 clusters in blackberries are very similar to those in solid U60 crystals, which supports the hypothesis that the linkages of POMs in blackberries are cation-mediated.

The SAXS data in the low- and mid-q region (<0.01 Å^{-1}) contain information about the sizes and shapes of blackberries in solution. However, identical scattering patterns may arise from blackberries with different size and shape distributions. The observed data show dramatic variations across the range of

DOI: 10.1021/jacs.5b09802
J. Am. Chem. Soc. 2016, 138, 191−198

added cations (Figure 2). The observed variability and the difficulty in modeling and interpreting that variability prompted our efforts to image these systems using cryo-TEM.

Cryogenic Transmission Electron Microscopy. Isolated U60 clusters can be discerned in cryo-TEM images collected prior to significant assembly of blackberries (Figure 3). The sensitivity of the vitrified solution to electron beam damage prevented the collection of higher-resolution images, but the images are sufficient to identify individual clusters. Specifically, the image shows 2.5 nm U60 clusters spatially isolated from each other. The cluster size is consistent with the center-to-center distances obtained using SAXS.

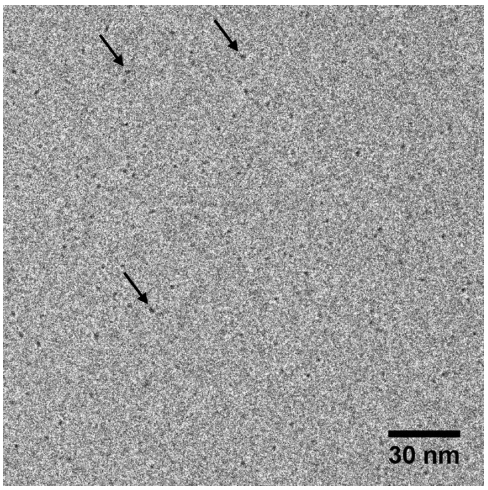

Figure 3. Cryo-TEM image of U60 nanoclusters vitrified before the addition of cations. Several nanoclusters are indicated by arrows to guide the eye.

Cryo-TEM images of U60 solutions vitrified at specified times after cation addition demonstrate that added nitrates of Na^+, K^+, Mg^{2+}, and Ca^{2+} quickly induced a change from isolated clusters (monomers) to secondary structures comprising tens to hundreds of individual clusters. The addition of divalent cations induced the formation of blackberries, while the addition of monovalent cations induced the formation of even larger, sometimes tertiary, structures.

In the case of the divalent cations, the blackberries grow larger as time progresses, which is inconsistent with the "direct jump" to equilibrium size hypothesized by Liu.[11] Figure 4 shows cryo-TEM images of samples vitrified at specified times after Mg^{2+} or Ca^{2+} addition. Each image is labeled with the added cation and time, in minutes, between cation addition and vitrification. In the image of Ca24, several blackberries appear to be touching. However, this image cannot discern the relative positions of the blackberries along the direction of the electron beam, so it is uncertain whether the blackberries are in contact with each other or at different heights with respect to the thickness of the film of vitrified water.

The relatively even contrast at the edge and center of each blackberry (Figure 4) is consistent with the hypothesis that these structures are hollow. Solid spheres would be expected to

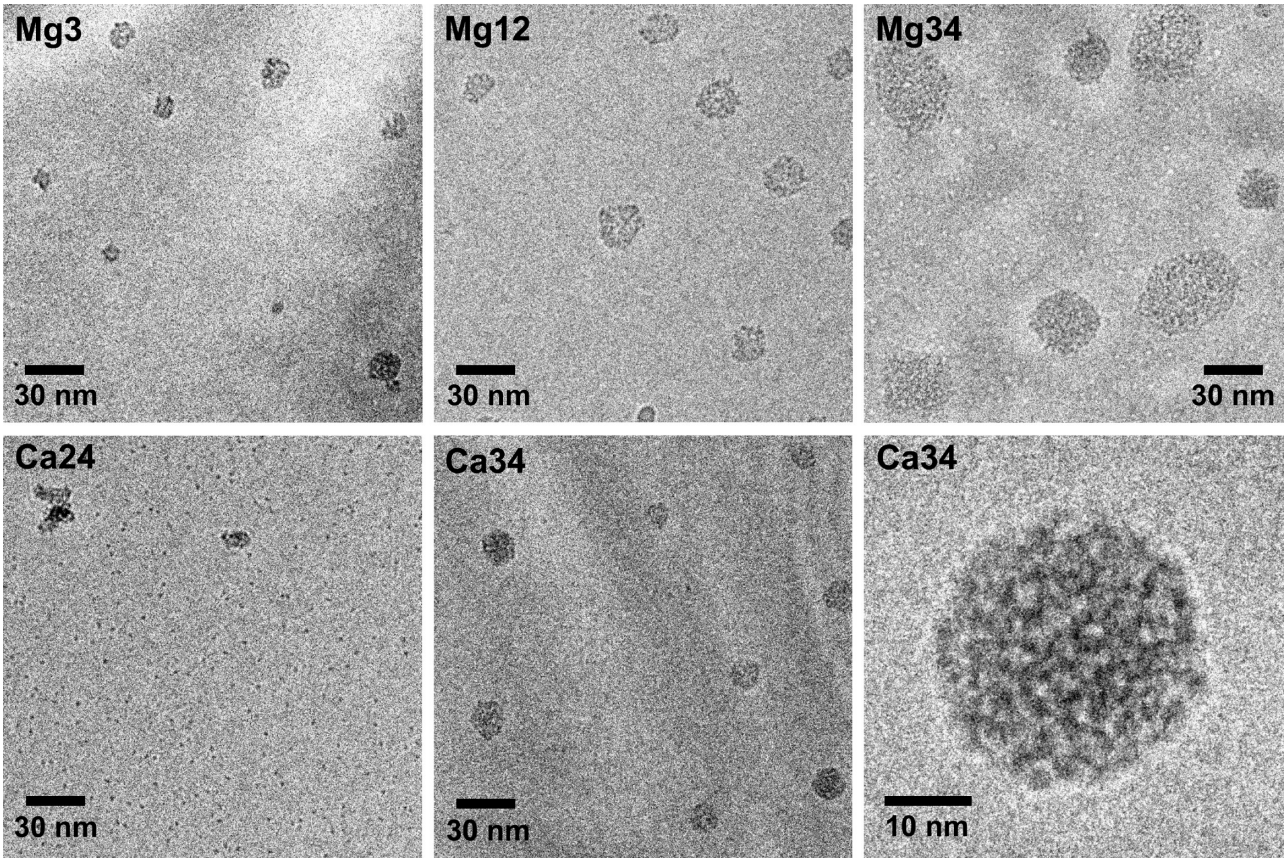

Figure 4. Cryo-TEM images of blackberries formed from U60 solutions vitrified after the addition of $Mg(NO_3)_2$ or $Ca(NO_3)_2$. Images are labeled with the cation added and the time, in minutes, between cation addition and vitrification.

DOI: 10.1021/jacs.5b09802
J. Am. Chem. Soc. 2016, 138, 191−198

have greater contrast at their centers due to increased mass/thickness contrast, whereas hollow spheres with dense walls would appear to have a "rind" in TEM images.[25] A TEM image of a circle with even contrast is consistent with round plates ("pancakes") or hollow spheres with less-dense walls. Tilting experiments demonstrated that the blackberries are roughly spherical (Figure S1), and we therefore conclude that they are hollow, which is in good agreement with models of POM blackberries previously reported.[12a,13,15,16]

The lower-right image in Figure 4 is representative of the secondary structures observed when divalent cations were added. This blackberry is about 32 nm × 32 nm and consists of an estimated 390 U60 clusters. Some individual U60 clusters can be discerned within the blackberry structures, particularly in smaller blackberries or near the edges of larger ones. Lighter gaps can be discerned between dark areas that correspond to individual clusters in the cryo-TEM images, as in Figures 3 and 4. These gaps presumably contain water and countercations that stabilize the assembly of clusters into larger structures, as discussed below.[16]

Though both of the divalent cations used induced the formation of blackberries, the blackberry size and rate of assembly were cation-dependent. Figure 5 shows the average

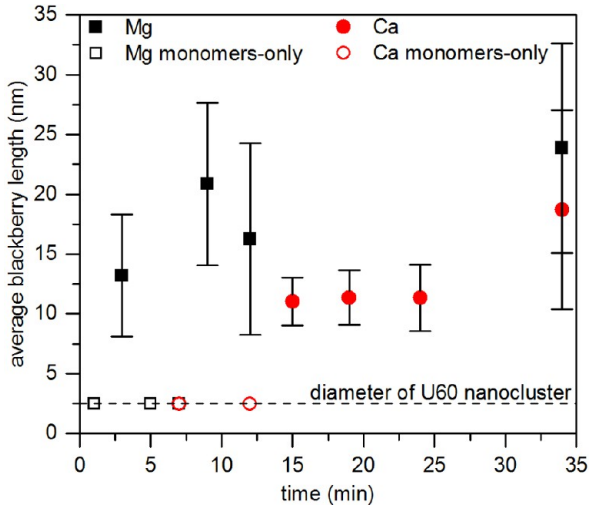

Figure 5. Average length of blackberries increases with time when Mg^{2+} or Ca^{2+} is added to a U60 solution. Blackberry length was measured from calibrated cryo-TEM images, and error bars represent the first standard deviation.

major axis length of the blackberries as a function of time. Mg-U60 blackberries formed more rapidly and were larger overall than Ca-U60 blackberries, and the difference in size after 34 min was statistically significant (p value $< 1 \times 10^{-7}$). Average blackberry aspect ratios ranged from 1.1 to 1.3 for both Mg-U60 and Ca-U60 and were independent of blackberry size. The dashed line at 2.5 nm corresponds to the diameter of individual U60 clusters; open symbols on this line indicate times at which images were collected but only U60 monomers were observed.

Interestingly, only monomers were seen in Mg-U60 samples vitrified 1 and 24 h after Mg^{2+} addition. We attribute this to settling of larger structures or precipitation of U60 onto the walls and bottom of the container, which was observed while preparing samples for SAXS measurements and is known to occur at the cation concentrations used here (above the critical salt concentration).[16]

In contrast to the quite spherical blackberries observed with addition of the divalent cations, sodium and potassium cations induced the formation of large, fractal-like tertiary structures. These results are at odds with previous reports describing the formation of spherical blackberries.[11,13,15] Here, a "tertiary structure" is defined as any large structure that can be outlined in a cryo-TEM image by two or more ellipses. We show later that in fact these structures may be tertiary structures assembled from blackberry building blocks.

Figure 6 shows cryo-TEM images in which primary, secondary, and tertiary structures can be discerned. At earlier stages of assembly, monomers and blackberries are observed (top row, images Na12 and K10). Some structures may have already reached a tertiary level of assembly, particularly those in the image labeled "K10" that appear to be composed of two or three blackberries. At later stages, the tertiary structures have increased in size and taken on a fractal-like appearance (Figure 6, bottom row, images Na28 and K15).

Mechanisms of Secondary and Tertiary Structure Formation. Assembly of transition metal (TM) POMs into blackberries occurs predominantly in systems of large POMs with low charge density,[9] criteria that are also met by U-POMs. The addition of cations to U60 solutions facilitates assembly into blackberries and tertiary structures, presumably through a cation-mediated mechanism.[13,16,26]

Lower net surface charge when divalent cations are added could explain why the blackberries observed in the Mg-U60 and Ca-U60 solutions were larger than those formed with monovalent cations. However, the Mg-U60 blackberries were larger than the Ca-U60 blackberries, which is inconsistent with the observation by Gao et al.[16] that cations with smaller hydrated sizes form larger blackberries (Mg^{2+} has a larger hydrated size than Ca^{2+}). While their study was also performed with 1 mg/mL U60 crystals in water, the concentrations of monovalent cations used were all below the critical salt concentration, so this may not be directly comparable to our work with divalent cations at concentrations above the critical salt concentration.

The formation of secondary and tertiary structures when monovalent cations were added was also cation-dependent. The average number of U60 clusters per tertiary structure is plotted as black squares in Figure 7. Error bars represent the smallest and largest clusters observed for each sample. Large tertiary structures, up to thousands of nanoclusters in size, were rapidly formed in solutions containing K^+. Tertiary structures in Na-U60 solutions formed more slowly and were smaller than those with K^+.

The fraction of nanoclusters residing in tertiary structures was determined by comparing the number of U60 nanoclusters residing in tertiary structures to the number of U60 clusters in secondary (blackberry) and tertiary structures combined (i.e., all nonmonomer clusters). These values are represented by gray bars in Figure 7. The average tertiary structure size did not directly correspond to the fraction of nanoclusters residing in tertiary structures. For example, the average structure size decreased in Na-U60 between 15 and 28 min, but the fraction of nanoclusters in tertiary structures increased over the same time period. This may indicate that the sedimentation of larger structures had begun as the remaining monomers were incorporated into smaller tertiary structures. Sedimentation is also likely in the 32 min sample, in which less than 20% of the nanoclusters were observed to reside in tertiary structures. Notably, 100% of U60 clusters resided in tertiary structures

DOI: 10.1021/jacs.5b09802
J. Am. Chem. Soc. 2016, 138, 191−198

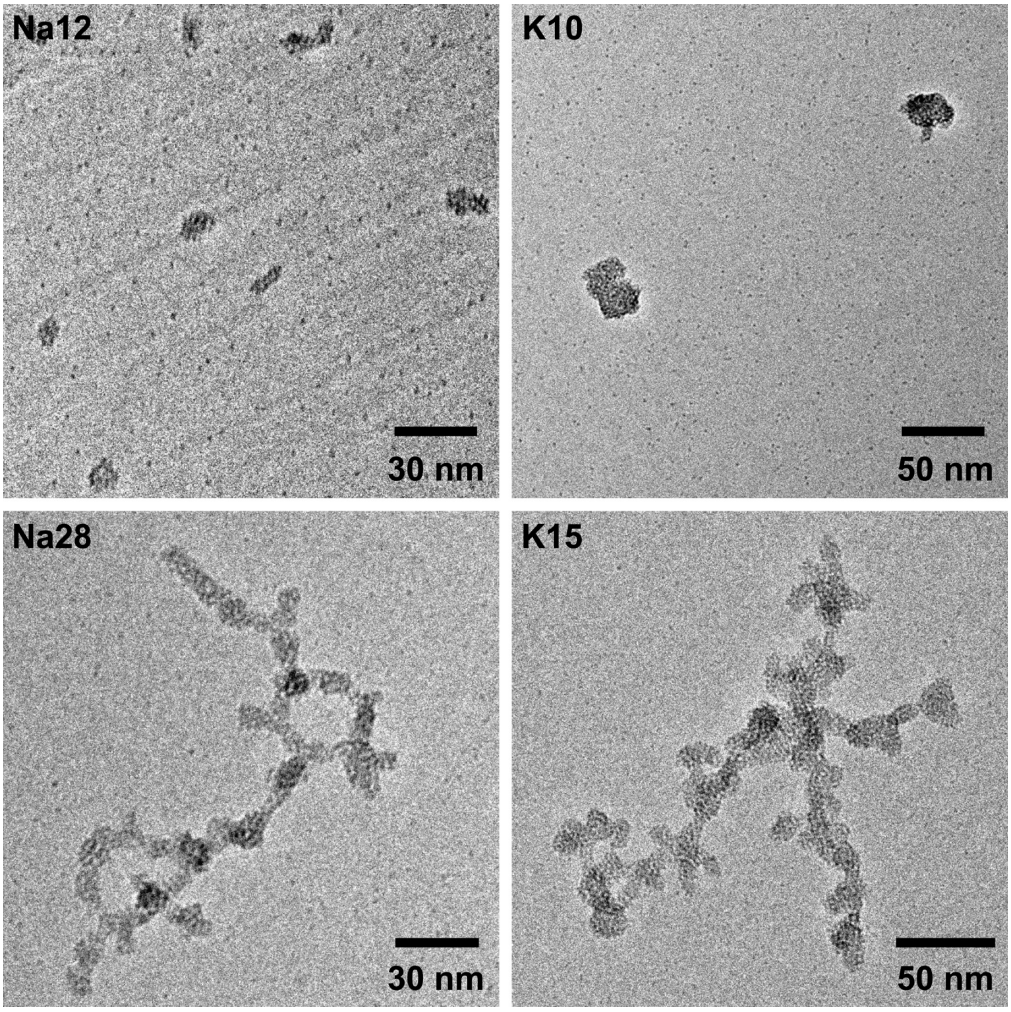

Figure 6. Cryo-TEM images of Na-U60 after 12 and 28 min and K-U60 after 10 and 15 min. Both cations induced the formation of small blackberries at early times that eventually grew into fractal-like structures. This is proposed to be a tertiary level of self-assembly.

only 15 min after addition of K^+. Small tertiary structures were also observed at a few sampling times for Mg-U60 and Ca-U60, but these structures did not persist and included less than 40% of the nonmonomer nanoclusters.

These data do not enable us to discern whether the tertiary structures are assembled from secondary blackberries or by monomer-by-monomer addition. Blackberry and tertiary structure assembly are dynamic processes, and cryo-TEM is only able to provide snapshots. The use of a real-time imaging technique such as fluid cell TEM would provide valuable insight into this process. Nevertheless, the available data support the hypothesis that the large structures observed in Na-U60 and K-U60 are tertiary assemblies based on blackberry secondary building blocks. A comparison of the average major axis length for isolated blackberries and those incorporated as secondary structural building blocks of the tertiary structures, plotted in Figure 8, shows that the two categories of blackberries are of similar size. The differences in average blackberry lengths between the two categories for each sample are statistically indistinguishable (all p values > 1), and the blackberries also have similar aspect ratios.

Finally, isolated U60 clusters were visible in all of the samples after the addition of Ca^{2+}, K^+, and Na^+, even in the presence of blackberries or tertiary structures. This indicates that either there was insufficient cation present to cause aggregation of all of the U60 clusters, that insufficient time transpired for complete aggregation, or perhaps that a steady state had been achieved between aggregation and disaggregation. With the exception of the sample vitrified after 3 min, which had both small blackberries and monomers, no isolated U60 clusters were observed in the presence of Mg-U60 blackberries.

In the presence of monovalent cations, the trends in blackberry and tertiary structure size are consistent with the dependence on hydrated cation size observed by Gao et al.,[16] who proposed that ions with smaller hydrated radii are preferred because they fit more easily into the available bonding sites on the nanoclusters. K^+, which has a smaller hydrated radius than Na^+, generally led to larger tertiary structures and larger blackberries (all p values statistically significant). Unlike in the work of Gao et al., blackberry and tertiary structure formation was observed after Na^+ was added to a U60 solution, which can be attributed to the much higher concentration of added cation.

Blackberry Formation without Added Cations. Figure 9 shows a cryo-TEM image of blackberries in a U60 solution that was not treated with additional cations but had simply been aged at high concentration (59 mg/mL). This is the first observation of U60 blackberries formed without addition of cations.[16] Imaging of the aged U60 solution revealed blackberries averaging 17.7 ± 10.4 nm in major axis length.

DOI: 10.1021/jacs.5b09802
J. Am. Chem. Soc. 2016, 138, 191−198

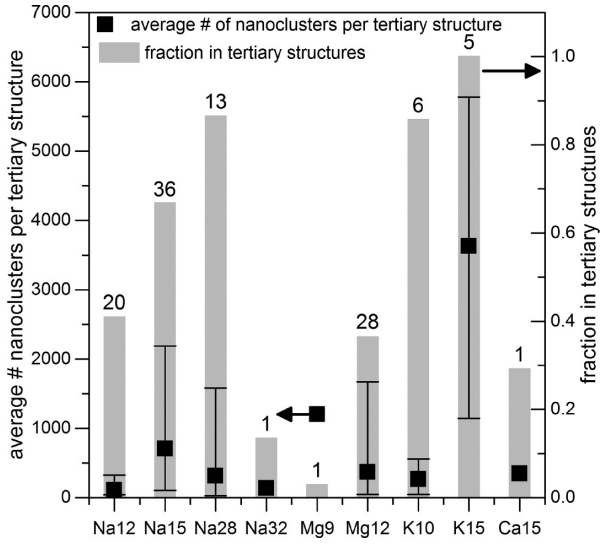

Figure 7. Left axis, black squares: The number of U60 nanoclusters per tertiary structure. Error bars show the smallest and largest tertiary structure observed in each sample and are omitted for samples in which only one tertiary structure was observed. The number of tertiary structures observed in each sample is indicated by the numbers above the gray bars. Right axis, gray bars: The fraction of U60 nanoclusters residing in tertiary structures relative to U60 nanoclusters residing in blackberries and tertiary structures combined. The number of nanoclusters in tertiary structures increases with time when group I cations are added. Tertiary structures are occasionally present in group II cation samples.

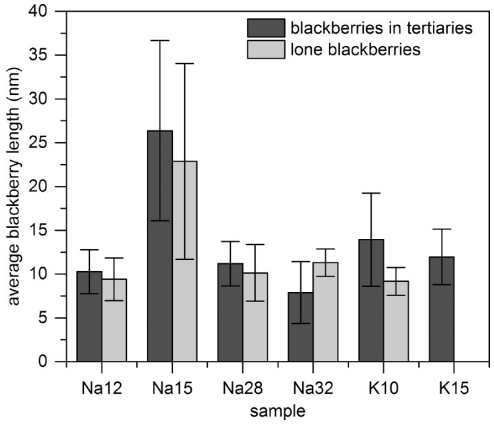

Figure 8. Comparison of major axis lengths in blackberries used as building blocks of tertiary structures (dark gray) and isolated blackberries not incorporated into tertiary structures (light gray). Samples are labeled with the cation added and the time, in minutes, between cation addition and vitrification. Within each pair of bars, the average sizes for the two types of blackberries were statistically indistinguishable. Error bars represent the first standard deviation. No isolated blackberries were observed in sample K15.

One possible explanation for the presence of these blackberries is a decrease in the interaction distance between U60 nanoclusters as the cluster concentration increases, which forces the nanoclusters closer together. The calculated effective charge drops as the U60 concentration increases,[16] which may facilitate the assembly of nanoclusters into blackberries, just as when cations are added to decrease nanocluster charge density. We hypothesize that, once formed, the blackberries are stable and do not disassemble upon dilution because of side-on

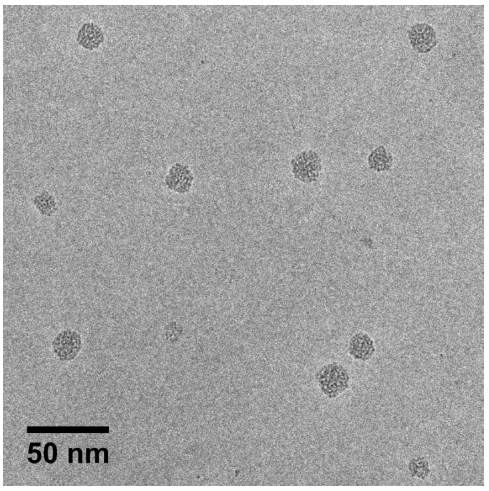

Figure 9. Cryo-TEM image of blackberries formed from a U60 solution (59 mg/mL) with no added cation aged at room temperature for 7 months and diluted to 1 mg/mL prior to vitrification.

bonding of cations between neighboring nanoclusters. Although extra cations were not added, Li^+ and K^+ present from the original synthesis may be available for cluster-to-cluster bonding.

Commentary on Representative Measurements. One of the major limitations of TEM is the vanishingly small amount of sample that can be imaged. A single high-resolution TEM image may contain only attograms of material,[27] and the average blackberry and fractal structure sizes are reported from the measurement of as few as 11 or as many as 355 blackberries and as few as one or as many as 36 tertiary structures. Conclusions about large populations based on such small sample sizes must be done with caution, and the use of complementary techniques such as SAXS and DLS can lend important insight into characteristics that are representative of a larger amount of sample.

CONCLUSION

Cryo-TEM has been used for the first time to image blackberries assembled from POMs in situ and to provide time-resolved insights into their formation. U60 nanoclusters are ideal for this type of study because they are stable, high-symmetry clusters with very high electron density, which provides for excellent contrast relative to the vitrified solvent. Images collected for aqueous solutions of U60 with various added cations indicate that U60 can be induced to self-assemble into secondary and tertiary structures. The addition of divalent cations produced hollow, near-spherical blackberry structures. The addition of monovalent cations yielded both blackberries and tertiary structures, with rates of inclusion of nanoclusters into tertiary structures as high as 100%. Both the kinetics of assembly and the size and morphology of the assembled structures depend on the identity of the cation. The images collected here have provided the size and shape of structures that have previously been analyzed only as averages of bulk samples.

Cryo-TEM is a promising technique for further studies of U-POM superstructures and any sample that is significantly altered by drying. Further work with techniques such as fluid cell TEM could also lend insight into the dynamics of U60 cluster assembly and answer questions about the reversibility of assembly, changes in blackberry size with time, and the

DOI: 10.1021/jacs.5b09802
J. Am. Chem. Soc. 2016, 138, 191−198

possibility of tertiary structure formation from blackberries versus direct assembly of monomers into fractal-like structures.

■ ASSOCIATED CONTENT

Supporting Information

The Supporting Information is available free of charge on the ACS Publications website at DOI: 10.1021/jacs.5b09802.

Tables of solution compositions for SAXS and TEM experiments, center-to-center distances calculated from SAXS measurements, and a series of cryo-TEM images of Ca34 blackberries at four tilt angles (PDF)

■ AUTHOR INFORMATION

Corresponding Authors

*rleepenn@umn.edu

*pburns@nd.edu

Present Address

[‖]J.A.S.: Physical and Computational Sciences Division, Pacific Northwest National Laboratory, Richland, WA 99352, United States.

Notes

The authors declare no competing financial interest.

■ ACKNOWLEDGMENTS

The participation of J.A.S. and R.L.P. in this research was funded by the National Science Foundation (0957696). J.A.S. also received funding from the University of Minnesota IPrime Nanostructural Materials and Processes Program. The participation of C.M.W. and P.C.B. in this research was funded by the Office of Basic Energy Sciences of the U.S. Department of Energy as part of the Materials Science of Actinides Energy Frontiers Research Center (DE-SC0001089). Parts of this work were carried out in the Characterization Facility at the University of Minnesota, a member of the NSF-funded Materials Research Facilities Network (www.mrfn.org) via the MRSEC Program. We gratefully acknowledge Jan Ilavsky at the Advanced Photon Source, Argonne National Laboratory, for his assistance with pinhole SAXS and USAXS measurements.

■ REFERENCES

(1) Burns, P. C.; Sigmon, G. E. *Uranium: Cradle to Grave*; Mineralogical Association of Canada: Québec, Canada, 2013; Vol. *43*, p 437.

(2) Abrefah, J.; Marschmann, S.; Jenson, E. D. *Examination of the Surface Coatings Removed from K-East Basin Fuel Elements*; PNNL-11806; Pacific Northwest National Laboratory: Richland, WA, 1998.

(3) (a) Finn, P. A.; Hoh, J. C.; Wolf, S. F.; Slater, S. A.; Bates, J. K. *Radiochim. Acta* **1996**, *74*, 65. (b) Bruno, J.; Ewing, R. C. *Elements* **2006**, *2*, 343. (c) Finch, R. J.; Buck, E. C.; Finn, P. A.; Bates, J. K. In *Scientific Basis for Nuclear Waste Management XXII*; Wronkiewicz, D. J., Lee, J. H., Eds.; Materials Research Society: Warrendale, PA, 1999; Vol. *556*, pp 431–438. (d) Gephart, R. E. *Hanford: A Conversation about Nuclear Waste and Cleanup*; Battelle Press: Richland, WA, 2003. (e) Girardot, C. L.; Harlow, D. G. Hanford Single-Shell Tank Leak Causes and Locations - 241-SX Farm PNNL RPP-RPT-54910, Rev. 0; Washington River Protection Solutions: Richland, WA, 2014.

(4) (a) Finch, R. J.; Ewing, R. C. *J. Nucl. Mater.* **1992**, *190*, 133. (b) Burns, P. C.; Ewing, R. C.; Navrotsky, A. *Science* **2012**, *335* (6073), 1184–8.

(5) (a) Qiu, J.; Burns, P. C. *Chem. Rev.* **2013**, *113* (2), 1097–120. (b) Burns, P. C. *Mineral. Mag.* **2011**, *75* (1), 1–25. (c) Sigmon, G. E.; Unruh, D. K.; Ling, J.; Weaver, B.; Ward, M.; Pressprich, L.; Simonetti, A.; Burns, P. C. *Angew. Chem., Int. Ed.* **2009**, *48* (15), 2737–2740.

(6) Flynn, S. L.; Szymanowski, J. E. S.; Gao, Y.; Liu, T.; Burns, P. C.; Fein, J. B. *Geochim. Cosmochim. Acta* **2015**, *156*, 94–105.

(7) Yin, P.; Li, D.; Liu, T. *Isr. J. Chem.* **2011**, *51* (2), 191–204.

(8) (a) Ammam, M. *J. Mater. Chem. A* **2013**, *1* (21), 6291. (b) Long, D. L.; Tsunashima, R.; Cronin, L. *Angew. Chem., Int. Ed.* **2010**, *49* (10), 1736–58.

(9) Nyman, M.; Burns, P. C. *Chem. Soc. Rev.* **2012**, *41* (22), 7354–7367.

(10) Muller, A.; Diemann, E.; Kuhlmann, C.; Eimer, W.; Serain, C.; Tak, T.; Knochel, A.; Pranzas, P. K. *Chem. Commun.* **2001**, *19*, 1928–1929.

(11) Liu, T. *Langmuir* **2010**, *26* (12), 9202–9213.

(12) (a) Pigga, J. M.; Teprovich, J. A.; Flowers, R. A.; Antonio, M. R.; Liu, T. *Langmuir* **2010**, *26*, 9449–9456. (b) Liu, G.; Liu, T. *Langmuir* **2005**, *21*, 2713–2720. (c) Liu, G.; Cai, Y.; Liu, T. *J. Am. Chem. Soc.* **2004**, *126*, 16690–16691.

(13) Kistler, M. L.; Bhatt, A.; Liu, G.; Casa, D.; Liu, T. *J. Am. Chem. Soc.* **2007**, *129*, 6453–6460.

(14) Liu, G.; Liu, T.; Mal, S. S.; Kortz, U. *J. Am. Chem. Soc.* **2006**, *128*, 10103–10110.

(15) Liu, T.; Diemann, E.; Li, H.; Dress, A. W. M.; Muller, A. *Nature* **2003**, *426* (6962), 59–62.

(16) Gao, Y.; Haso, F.; Szymanowski, J. E. S.; Zhou, J.; Hu, L.; Burns, P. C.; Liu, T. *Chem. - Eur. J.* **2015**, *21* (51), 18785–18790.

(17) Chen, B.; Jiang, H.; Zhu, Y.; Cammers, A.; Selegue, J. P. *J. Am. Chem. Soc.* **2005**, *127* (12), 4166–4167.

(18) Zhu, Y.; Cammers-Goodwin, A.; Zhao, B.; Dozier, A.; Dickey, E. C. *Chem. - Eur. J.* **2004**, *10* (10), 2421–2427.

(19) (a) Yuwono, V.; Burrows, N. D.; Soltis, J. A.; Penn, R. L. *J. Am. Chem. Soc.* **2010**, *132*, 2163–2165. (b) Yuwono, V. M.; Burrows, N. D.; Soltis, J. A.; Anh Do, T.; Lee Penn, R. *Faraday Discuss.* **2012**, *159* (1), 235–245. (c) Wang, C.-Y.; Böttcher, C.; Bahnemann, D. W.; Dohrmann, J. K. *J. Nanopart. Res.* **2004**, *6*, 119–122. (d) Klokkenburg, M.; Vonk, C.; Claesson, E. M.; Meeldijk, J. D.; Erné, B. H.; Philipse, A. P. *J. Am. Chem. Soc.* **2004**, *126* (51), 16706–16707. (e) Legg, B. A.; Zhu, M.; Comolli, L. R.; Gilbert, B.; Banfield, J. F. *Langmuir* **2014**, *30*, 9931–9940.

(20) (a) Berret, J.-F.; Schonbeck, N.; Gazeau, F.; El Kharrat, D.; Sandre, O.; Vacher, A.; Airiau, M. *J. Am. Chem. Soc.* **2006**, *128* (5), 1755–1761. (b) Legg, B. A.; Zhu, M.; Comolli, L. R.; Gilbert, B.; Banfield, J. F. *Environ. Sci. Technol.* **2014**, *48* (23), 13703–13710.

(21) Ilavsky, J.; Jemian, P. R.; Allen, A. J.; Zhang, F.; Levine, L. E.; Long, G. G. *J. Appl. Crystallogr.* **2009**, *42*, 469–479.

(22) Ilavsky, J.; Jemian, P. R. *J. Appl. Crystallogr.* **2009**, *42* (2), 347–353.

(23) Rasband, W. S. *ImageJ*; U. S. National Institutes of Health: Bethesda, MD, 1997–2015.

(24) Mackay, A. L.; Finney, J. L.; Gotoh, K. *Acta Crystallogr., Sect. A: Cryst. Phys., Diffr., Theor. Gen. Crystallogr.* **1977**, *33* (1), 98–100.

(25) Williams, D. B.; Carter, C. B. *Transmission Electron Microscopy: A Textbook for Materials Science*; Plenum Press: New York, 1996.

(26) Pigga, J. M.; Kistler, M. L.; Shew, C.-Y.; Antonio, M. R.; Liu, T. *Angew. Chem., Int. Ed.* **2009**, *48*, 6538–6542.

(27) Penn, R. L.; Soltis, J. A. *CrystEngComm* **2014**, *16* (8), 1409–1418.

DOI: 10.1021/jacs.5b09802
J. Am. Chem. Soc. 2016, 138, 191–198